Redox Biology 53 (2022) 102338

Contents lists available at ScienceDirect

Redox Biology

journal homepage: www.elsevier.com/locate/redox

Mitigation of doxorubicin-induced cardiotoxicity with an H_2O_2-Activated, H_2S-Donating hybrid prodrug

Qiwei Hu [a,1], Rama D. Yammani [b,1], Heather Brown-Harding [c], David R. Soto-Pantoja [d], Leslie B. Poole [b,*], John C. Lukesh III [a,**]

[a] Department of Chemistry, Wake Forest University, Wake Downtown Campus, Winston-Salem, NC, 27101, USA
[b] Department of Biochemistry, Wake Forest School of Medicine, Winston-Salem, NC, 27157, USA
[c] Department of Biology, Wake Forest University, Winston-Salem, NC, 27109, USA
[d] Department of Cancer Biology and Department of Surgery/Hypertension, Wake Forest School of Medicine, Winston-Salem, NC, 27157, USA

ARTICLE INFO

Keywords:
Cardiotoxicity
Chemotherapeutic
Doxorubicin
Hydrogen sulfide
Hydrogen peroxide

ABSTRACT

Doxorubicin (DOX) is one of the most effective anticancer agents in clinical oncology. Its continued use, however, is severely limited by its dose-dependent cardiotoxicity which stems, in part, from its overproduction of reactive oxygen species (ROS) and often manifests itself as full-blown cardiomyopathy in patients, years after the cessation of treatment. Therefore, identifying DOX analogs, or prodrugs, with a diminished cardiotoxic profile is highly desirable. Herein, we describe a novel, H_2O_2-responsive DOX hybrid codrug (mutual prodrug) that has been rationally designed to concurrently liberate hydrogen sulfide (H_2S), a purported cardioprotectant with anticancer activity, in an effort to maintain the antitumor effects of DOX while simultaneously reducing its cardiotoxic side effects. Experiments with cardiomyoblast cells in culture demonstrated a rapid accumulation of prodrug into the cells, but diminished apoptotic effects compared with DOX, dependent upon its release of H_2S. Cells treated with the prodrug exhibited significantly higher Nrf2 activation relative to DOX-treated cells. Preliminary indications, using a mouse triple-negative breast cancer cell line sensitive to DOX treatment, are that the prodrug maintains considerable toxicity against the tumor-inducing cell line, suggesting significant promise for this prodrug as a cardioprotective chemotherapeutic to replace DOX.

1. Introduction

Anthracycline antibiotics are a family of compounds that have displayed promising antineoplastic properties since their discovery in the 1960s (Fig. 1) [1]. Doxorubicin (DOX) is one of the most prominent members of this class and is among the most effective anticancer drugs ever discovered [2,3]. Even with advancements in targeted therapy on the rise, DOX has endured as one of the most integral oncology drugs in modern medicine and is routinely employed in highly successful combination drug therapies for the treatment of breast cancer, solid tumors, soft tissue sarcomas, leukemias, and aggressive lymphomas [4].

The anticancer effects of DOX have been explored in detail and several mechanisms have been proposed, including intercalation of double-stranded DNA, stabilization of topoisomerase II α–DNA cleavage complex, and the generation of reactive oxygen species (ROS) [5]. Despite its success in increasing survival rates of cancer patients, the continued clinical use of DOX is severely hampered by its cardiotoxic side effects [6]. While DOX does exhibit acute cardiotoxicity, its chronic, dose-dependent form is far more concerning, with DOX-induced cardiomyopathy and congestive heart failure often emerging in patients 4–20 years after the cessation of therapy [7,8]. Although a precise mechanism of DOX-mediated cardiotoxicity has yet to be defined, much evidence points to its uncontrolled production of ROS as a primary culprit [9–13].

Like all anthracyclines, the chemical structure of DOX renders it predisposed to the production of ROS since its quinone moiety is highly susceptible to enzyme-mediated, one electron reductions. Enzymes responsible for facilitating this chemistry include complex I of the mitochondrial electron transport chain, which transforms DOX into a semiquinone that can rapidly reduce molecular oxygen to regenerate

* Corresponding author.
** Corresponding author.
E-mail addresses: lbpoole@wakehealth.edu (L.B. Poole), lukeshjc@wfu.edu (J.C. Lukesh).
[1] These authors contributed equally to this work.

https://doi.org/10.1016/j.redox.2022.102338
Received 2 March 2022; Received in revised form 2 May 2022; Accepted 11 May 2022
Available online 16 May 2022

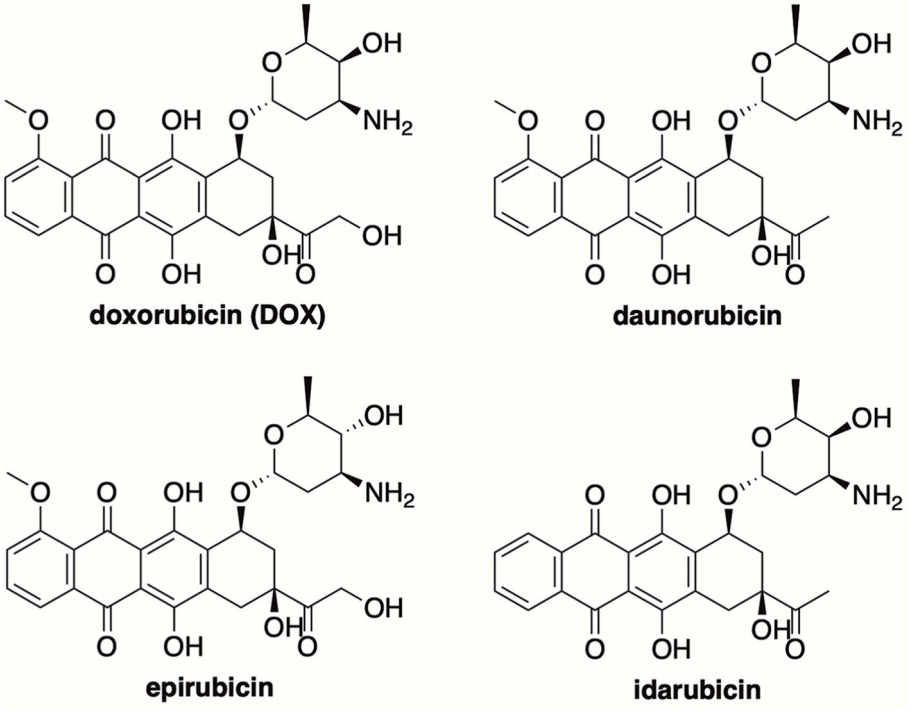

Fig. 1. Anthracycline antibiotics.

DOX while producing superoxide in the process [14]. DOX's quinone–semiquinone redox cycling is known to generate superfluous levels of superoxide, which subsequently gives rise to other reactive oxygen and nitrogen species. Moreover, DOX displays a high binding affinity for cardiolipin, a 4-acyl chain phospholipid that exists exclusively in the inner mitochondrial membrane, which concentrates the drug within this subcellular space [15]. Both factors facilitate the production of ROS, which results in significant cellular damage to lipids, proteins, and DNA. Due to its increased mitochondrial density and poor antioxidant defense relative to other organs and tissues, the heart is especially prone to oxidative injury, providing a basis for DOX-induced cardiomyopathy [10,16].

Various strategies have been explored in an effort to reduce the cardiotoxic side effects of DOX. One promising approach is to administer antioxidants alongside DOX to counter its ROS-production [17–19]. Designs that directly link an antioxidant payload to DOX have also been explored [20]. To this end, it has recently been shown that linking DOX to various hydrogen sulfide-releasing scaffolds results in analogs endowed with reduced cardiotoxicity [21].

Hydrogen sulfide (H_2S) is an endogenous signaling molecule that mediates numerous physiological and pathophysiological processes within the human body [22–24]. Specifically, H_2S has been shown to provide numerous beneficial effects on the cardiovascular system. As a smooth muscle relaxant, H_2S plays a pivotal role in reducing blood pressure [25,26]. Further studies have attributed this effect to the activation of K_{ATP} channels via H_2S-mediated protein persulfidation, which hyperpolarizes and relaxes smooth muscle [27,28]. In addition to its vasorelaxant properties, H_2S has been shown to exert additional positive effects on the cardiovascular system, including the attenuation of myocardial reperfusion injury and the promotion of angiogenesis [29–31]. Moreover, given its potent antioxidant properties, H_2S has been shown to provide cellular protection against hydrogen peroxide (H_2O_2) and other ROS, whose excess production is linked to inflammation, oxidative stress, and cardiovascular injury [32–34].

As a general approach to improving the therapeutic index of drugs, various prodrug strategies are often investigated. In more recent years, ROS-inducible anticancer prodrugs have emerged as a promising design [35]. Due to increased metabolic activity and mitochondrial dysfunction, cancer cells are known to exhibit elevated levels of ROS [36]. This feature has been exploited in the development of ROS-activated prodrugs of SN-38, nitrogen mustards, 5-fluorouracil, and doxorubicin, resulting in promising tumor-selective agents [37–40].

Motivated by these earlier reports, we describe a novel DOX hybrid prodrug (**c1**, Fig. 2A) that has been rationally designed to concurrently liberate both hydrogen sulfide (by way of COS hydrolysis) [41,42] and doxorubicin in response to elevated levels of ROS (Fig. 2B). To the best of our knowledge, this is the first design that imparts both tumor-selective activation and H_2S delivery as a synergistic strategy to combat DOX-induced cardiotoxicity. This unique combination was shown to afford impressive cardioprotective effects in H9C2 (rat cardiomyoblast) cells while maintaining the antitumor activity of DOX in 4T1 (mouse triple-negative breast cancer) cells.

2. Materials and methods

2.1. General chemistry

Commercial reagents were used without further purification unless stated otherwise. Dichloromethane and tetrahydrofuran (THF) were dried over a column of alumina. Flash chromatography was performed with columns of 40–63 Å silica from Silicycle (Québec City, Canada). Thin-layer chromatography (TLC) was performed on plates of EMD 250 μm silica 60-F_{254}. The term "concentrated under reduced pressure" refers to removing solvents and other volatile materials using a rotary evaporator while maintaining the water-bath temperature below 40 °C. Residual solvent was removed from samples at high vacuum (<0.1 torr) using an Edwards RV5 pump. Analytically pure samples of final products were accessed using an Agilent (Santa Clara, CA) preparative HPLC, equipped with a C18 reverse-phase preparative column, diode array detector, and fraction collector. Liquid Chromatography-Mass Spectrometry (LC-MS) analyses were performed using a Bruker AmaZon SL with a Shimadzu SPD-M20A UV detector and a Shimadzu LC-20AB pump, equipped with an analytical C18 column (Agilent Technologies, SB-C18 Analytical HPLC Col. 4.6 × 150). All NMR spectra were acquired

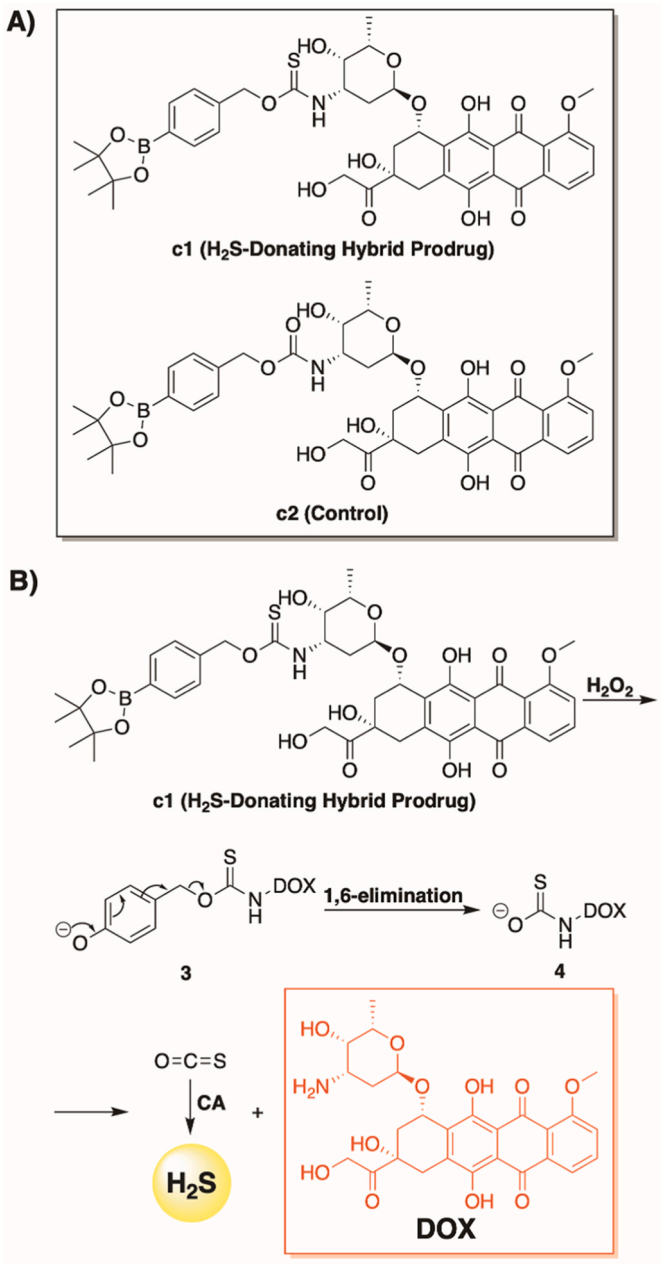

Fig. 2. Prodrug structures and H_2O_2-dependent release pathway, (A) Prodrugs assessed in this study. (B) Proposed mechanism for the simultaneous release of H_2S and DOX from c1 in response to H_2O_2. CA = carbonic anhydrase.

at ambient temperature with a Bruker Ascend™ 400 MHz spectrometer and referenced to TMS or residual protic solvent. High-resolution mass spectra were acquired using a Thermo Orbitrap LTQ XL (ESI). Carbonyl sulfide liberation was detected using an Agilent 7890 GC/5975 MS with autosampler. Absorbance measurements for the methylene blue assay were taken with a Cary 100 UV–Vis spectrophotometer (Agilent). All data fitting was done with Prism 7 (GraphPad Software, La Jolla, Ca).

2.2. Chemical synthesis (see Scheme S1)

Potassium *tert*-butoxide (1.5 mL, 1 M in THF) was added dropwise to a solution of 4-(hydroxymethyl)phenylboronic acid pinacol ester (234 mg, 1.0 mmol) in dry CH_2Cl_2 (5 mL). The reaction mixture was then taken up with a syringe and added dropwise over a period of 5 min to a solution of di(2-pyridyl) thionocarbonate (464 mg, 2.0 mmol) dissolved in dry CH_2Cl_2 (5 mL). After reacting for 15 min under N_2(g), the reaction was confirmed to be complete by TLC, and the reaction mixture was diluted with CH_2Cl_2, washed with 1 M HCl(aq), dried over anhydrous $MgSO_4$, and concentrated under reduced pressure. Flash chromatography (15% v/v EtOAc in Hexanes) was used to isolate **1** (185 mg) in a 50% yield.

^{1}H NMR (400 MHz, Chloroform-d) δ 7.83 (d, J = 8.1 Hz, 2H), 7.60 (ddd, J = 7.2, 2.1, 1.3 Hz, 1H), 7.48 (d, J = 8.1 Hz, 2H), 7.26 (ddd, J = 9.5, 6.5, 2.1 Hz, 1H), 6.49 (dt, J = 9.5, 1.3 Hz, 1H), 6.12 (ddd, J = 7.2, 6.5, 1.3 Hz, 1H), 5.66 (s, 2H), 1.33 (s, 12H); **^{13}C NMR (101 MHz, Chloroform-d)** δ 192.6, 160.1, 140.1, 136.5, 135.4, 135.2, 127.8, 122.8, 105.7, 84.0, 76.8, 25.0; **ESI-MS** calculated for $[C_{19}H_{23}BNO_4S]^+$ $(M + H)^+$ requires m/z = 372.14, found 372.19.

To a stirred solution of doxorubicin hydrochloride (58 mg, 0.1 mmol) in dry DMF (1 mL) was slowly added a mixture of **1** (37 mg, 0.1 mmol) and Et_3N (200 μL, 1.4 mmol) in dry DMF (2 mL). The mixture was then left to react at room temperature, in the dark, and under an N_2(g) atmosphere. After stirring for 2 h, the reaction mixture was concentrated under reduced pressure and purified via flash chromatography (10% v/v MeOH in DCM) to isolate **c1** (78 mg, 95%). An analytically pure sample of **c1** (42 mg, 51%) was then obtained via HPLC (Agilent) using a C18 preparatory column and eluting at 20 mL/min with water (0–1 min), followed by a linear gradient (0–100% v/v) of acetonitrile/water (1–9 min), and finishing with an acetonitrile wash (9–12 min).

^{1}H NMR (400 MHz, Chloroform-d) δ 14.01 (s, 1H), 13.26 (s, 1H), 8.05 (dd, J = 7.7, 1.1 Hz, 1H), 7.81–7.77 (m, 3H), 7.41–7.38 (m, 1H), 7.33 (d, J = 8.1 Hz, 2H), 6.64 (d, J = 8.6 Hz, 1H), 5.55–5.52 (m, 1H), 5.42 (d, J = 2.3 Hz, 1H), 5.37–5.34 (m, 1H), 4.80 (d, J = 4.7 Hz, 2H), 4.62 (s, 1H), 4.56–4.49 (m, 1H), 4.21–4.16 (m, 1H), 4.09 (s, 3H), 3.79-3.77 (m, 1H), 3.49 (s, 2H), 3.35–3.27 (m, 1H), 3.00 (t, J = 4.7 Hz, 1H), 2.38–2.31 (m, 1H), 2.22–2.17 (m, 1H), 2.09–2.04 (m, 1H), 1.92–1.86 (m, 1H), 1.78 (td, J = 13.1, 4.1 Hz, 1H), 1.34 (s, 3H), 1.33 (s, 12H); **^{13}C NMR (101 MHz, Chloroform-d)** δ 214.1, 189.3, 187.3, 186.9, 161.2, 156.3, 155.9, 138.8, 135.9, 135.7, 135.1, 133.9, 133.7, 127.6, 126.9, 121.1, 120.0, 118.6, 111.8, 111.7, 100.3, 84.0, 71.9, 69.2, 69.0, 67.4, 65.8, 56.9, 53.6, 51.2, 35.9, 34.3, 29.1, 25.0, 17.0. HRMS calculated for $[C_{41}H_{46}O_{14}NBNaS]^+$ $(M + Na^+)$ requires m/z = 842.2630, found 842.2632. Purity of **c1** (retention time 12.5 min) was determined by LC-MS (Shimadzu) using a C18 analytical column and eluting at 0.4 mL/min with a linear gradient (20–90% v/v) MeOH/H_2O (0–2 min), followed by 90% v/v MeOH/H_2O (2–20min) and found to be >95% pure.

4-Nitrophenyl chloroformate (280 mg, 1.4 mmol) was dissolved in dry THF (5 mL) under an N_2(g) atmosphere. Next, a mixture of 4-(hydroxymethyl)phenylboronic acid pinacol ester (234 mg, 1.0 mmol), DMAP (48 mg, 0.4 mmol), and Et_3N (560 μL, 4.0 mmol) in dry THF (5 mL) was added dropwise. After stirring at room temperature for 4 h, the reaction mixture was concentrated under reduced pressure, diluted with EtOAc, washed with 1 M HCl(aq), dried over anhydrous $MgSO_4$, and rotary evaporated to dryness. Flash chromatography (15% v/v EtOAc in Hex) was used to isolate **2** (288 mg, 72%).

^{1}H NMR (400 MHz, Chloroform-d) δ 8.25 (d, J = 9.2 Hz, 2H), 7.85 (d, J = 8.1 Hz, 2H), 7.43 (d, J = 8.1 Hz, 2H), 7.37 (d, J = 9.2 Hz, 2H), 5.30 (s, 2H), 1.35 (s, 12H); **^{13}C NMR (101 MHz, Chloroform-d)** δ 155.6, 152.5, 145.5, 137.2, 135.3, 127.7, 125.4, 121.9, 84.1, 70.9, 24.9. MS (ESI): calcd for $C_{20}H_{22}BNNaO_7^+$ $(M + Na)^+$ 422.1382, found 422.21.

To a stirred solution of doxorubicin hydrochloride (58 mg, 0.1 mmol) in 1 mL of dry DMF was slowly added a mixture of **2** (40 mg, 0.1 mmol), DMAP (5 mg, 0.04 mmol), and Et_3N (20 μL, 0.14 mmol) in DMF (2 mL). The mixture was then left to react at room temperature, in the dark, and under an N_2(g) atmosphere. After reacting for 2 h, the solvent was then removed via rotary evaporation, and flash chromatography (10% v/v MeOH in DCM) was used to isolate **c2** (75 mg, 94%). An analytically pure sample of **c2** (33 mg, 41%) was then obtained via HPLC (Agilent) using a C18 preparatory column and eluting at 20 mL/min with water (0–1 min), followed by a linear gradient (0–100% v/v) of acetonitrile/water (1–9 min), and finishing with an acetonitrile wash (9–12 min).

^{1}H NMR (400 MHz, Chloroform-d) δ 13.97 (s, 1H), 13.23 (s, 1H), 8.03 (d, J = 7.8 Hz, 1H), 7.84–7.75 (m, 3H), 7.39 (d, J = 8.6, 1.1 Hz, 1H), 7.29 (d, J = 7.6 Hz, 2H), 5.50 (d, J = 3.9 Hz, 1H), 5.18–5.09 (m, 1H), 5.04 (s, 2H), 4.80–4.70 (m, 2H), 4.54 (s, 1H), 4.15–4.11 (m, 1H), 4.08 (s, 3H), 3.95–3.77 (m, 1H), 3.71–3.62 (m, 1H), 3.48 (s, 1H), 3.27 (dd, J = 17.0, 1.9 Hz, 1H), 3.09–2.92 (m, 2H), 2.33 (dt, J = 14.7, 2.1 Hz, 1H), 2.23–2.10 (m, 1H), 2.03–1.83 (m, 2H), 1.77 (td, J = 13.2, 4.1 Hz, 1H), 1.63 (s, 3H), 1.32 (s, 12H); **^{13}C NMR (101 MHz, Chloroform-d)** δ 214.0, 187.3, 186.9, 161.2, 156.3, 155.8, 155.6, 139.5, 135.9, 135.7, 135.1, 133.7, 127.3, 121.0, 120.0, 118.6, 111.8, 111.6, 100.8, 84.0, 69.7, 67.4, 66.8, 65.7, 56.8, 53.6, 47.1, 35.8, 34.2, 30.3, 29.8, 25.0, 22.8, 17.0, 14.3; HRMS calculated for $[C_{41}H_{46}O_{15}NBNa]^+$ (M + Na^+) requires m/z = 826.2858, found 826.2868. Purity of **c2** (retention time 11.7 min) was determined by LC-MS (Shimadzu) using a C18 analytical column and eluting at 0.4 mL/min with a linear gradient (20–90% v/v) MeOH/H_2O (0–2 min), followed by 90% v/v MeOH/H_2O (2–20min) and found to be >95% pure.

2.3. H_2S calibration curve using the methylene blue (MB) assay

2.3.1. (With carbonic anhydrase) Six separate vials were each filled with 150 μL of freshly degassed PBS (pH 7.4) containing $Zn(OAc)_2$ (2 mM), carbonic anhydrase (0.1 mg/mL), and DOX (80 μM). Next, 150 μL of Na_2S stock solution in freshly degassed PBS (pH 7.4), and at differing concentrations (6.25, 12.5, 25.0, 50.0, 100 and 200.0 μM), was added to each vial to give a final volume of 300 μL and a final concentration of 3.125, 6.25, 12.5, 25.0, 50.0, and 100.0 μM Na_2S. Next, 600 μL of MB cocktail (300 μL $FeCl_3$ (30.0 mM in 1.20 M HCl) and 300 μL N,*N*-dimethyl-*p*-phenylene diamine (20.0 mM in 7.20 M HCl)) was added to each vial and allowed to react for 30 min in the dark. The MB solution was transferred to a 1.0 mL UV cuvette and the absorbance at 670 nm was recorded (Fig. S1).

2.3.2. (Without carbonic anhydrase.) Six separate vials were each filled with 150 μL of freshly degassed PBS (pH 7.4) containing $Zn(OAc)_2$ (2 mM) and DOX (80 μM). Next, 150 μL of Na_2S stock solution in freshly degassed PBS buffer (pH 7.4), and at differing concentrations (6.25, 12.5, 25.0, 50.0, 100 and 200.0 μM), was added to each vial to give a final volume of 300 μL and a final concentration of 3.125, 6.25, 12.5, 25.0, 50.0, and 100.0 μM Na_2S. Next, 600 μL of MB cocktail (300 μL $FeCl_3$ (30.0 mM in 1.20 M HCl) and 300 μL N,*N*-dimethyl-*p*-phenylene diamine (20.0 mM in 7.20 M HCl)) was added to each vial and allowed to react for 30 min in the dark. The MB solution was transferred to a 1.0 mL UV cuvette and the absorbance at 670 nm was recorded (Fig. S2).

2.4. Time-dependent H_2S release from c1

A 10 mM stock solution of **c1** (or **c2**) was prepared in DMSO immediately prior to use. Hydrogen peroxide (H_2O_2, 10 mM) was prepared in freshly degassed PBS (pH 7.4). Carbonic anhydrase (CA) was prepared as 10 mg/mL in PBS buffer (pH 7.4), $Zn(OAc)_2$ (100 mM) was prepared in distilled water), and methylene blue cocktail was prepared as follows: $FeCl_3$ (20 mM, 1.2 M HCl) and *N*,*N*-dimethyl-*p*-phenylene diamine (20 mM, 7.2 M HCl).

2.4.1. (With carbonic anhydrase.) To a 20 mL scintillation vial containing 9770 μL of freshly degassed PBS (pH 7.4) was added stock solutions of carbonic anhydrase (50 μL), H_2O_2 (40 μL), $Zn(OAc)_2$ (100 μL), and **c1** (or **c2**) (40 μL). The resulting mixture was then stirred at 37 °C, and at various time points (1 min, 10 min, 20 min, 30 min, 40 min, 50 min, 60 min, 75 min, 90 min, 105 min, 120 min), a 300 μL aliquot was removed and added to the MB solution (300 μL $FeCl_3$ and 300 μL N,*N*-dimethyl-*p*-phenylene diamine). After reacting for 30 min in the dark, absorbance measurements were recorded at 670 nm.

2.4.2. (Without carbonic anhydrase) To a 20 mL scintillation containing 9820 μL of freshly degassed PBS (pH 7.4) was added stock solutions of H_2O_2 (40 μL), $Zn(OAc)_2$ (100 μL), and **c1** (or **c2**) (40 μL). The resulting mixture was then stirred at 37 °C, and at various time points (1 min, 10 min, 20 min, 30 min, 40 min, 50 min, 60 min, 75 min, 90 min, 105 min, 120 min), a 300 μL aliquot was removed and added to the MB solution (300 μL $FeCl_3$ and 300 μL N,*N*-dimethyl-*p*-phenylene diamine). After reacting for 30 min in the dark, absorbance measurements were recorded at 670 nm.

2.5. Time-dependent dox release from c1

A stock solution of **c1** (or **c2,** 10 mM) in DMSO and H_2O_2 (10 mM) in ammonium bicarbonate buffer (0.1 M, pH 7.4) were prepared immediately prior to use. To a 20 mL scintillation vial containing ammonium bicarbonate buffer (9980 μL) was then added H_2O_2 (10 μL) and **c1** (10 μL), and the reaction mixture was stirred at 37 °C. At various time points (0 min, 10 min, 35 min, 60 min, 80 min, 100 min, 120 min), a 1 mL (inject volume 60 μL) aliquot was removed and analyzed by LC-MS (using a C18 analytical column and eluting at 0.4 mL/min with a linear gradient (20–90% v/v) MeOH/H_2O (0–2 min), followed by 90% v/v MeOH/H_2O (2–19min)). The signals in the chromatogram were recorded at 500 nm and the peak corresponding to free DOX (7.0 min) was integrated. A calibration was generated and used to determine the concentration of released DOX from **c1** (or **c2**) at each time point.

2.6. Selectivity studies for DOX release from c1

Analyte stock solutions of glutathione (10 mM), oxidized glutathione (10 mM), homocysteine (10 mM), L-cysteine (10 mM), sodium nitrite ($NaNO_2$ 10 mM), superoxide (KO_2, 10 mM), sodium peroxynitrite (NaOONO, 10 mM), and sodium hypochlorite (NaClO, 10 mM), were prepared in ammonium bicarbonate buffer (0.1 M pH 7.4). To a 20 mL scintillation vial was then added 9980 μL of ammonium bicarbonate buffer (pH 7.4) and10 μL of analyte and **c1** stock solutions, and the resulting mixture was stirred at 37 °C. After reacting for 80 min, a 1 mL (inject volume 60 μL) aliquot was removed and analyzed by LC-MS (using a C18 analytical column and eluting at 0.4 mL/min with a linear gradient (20–90% v/v) MeOH/H_2O (0–2 min), followed by 90% v/v MeOH/H_2O (2–19min)). The signals in the chromatogram were recorded at 500 nm and the peak corresponding to free DOX (7.0 min) was integrated.

2.7. Cell culture

H9C2 rat cardiac myoblast cells were obtained from ATCC (CRL-1446, TIB-71). 4T1 mouse breast cancer cells were a gift to D.S.-P. from Dr. Patricia Steeg [National Cancer Institute (NCI, National Institutes of Health (NIH) Bethesda, Maryland). H9C2 cells were cultured in DMEM supplemented with 10% fetal bovine serum (FBS) penicillin/streptomycin, and glutamine kept at 37 °C and 5% CO_2. 4T1 cells were cultured in RPMI 1640 medium supplemented with 10% fetal bovine serum (FBS) penicillin/streptomycin, and glutamine kept at 37 °C and 5% CO_2.

2.8. Confocal microscopy

To evaluate drug uptake, H9C2 cells were plated at a density of 20,000 per well on 24 well #1.5 polymer chambered coverslips (Ibidi) in media including 10% FBS and allowed to adhere for ~20 h. Prior to imaging analysis, the media was replaced with Fluorobrite DMEM imaging media (Gibco) supplemented with 5% FBS. To 1 mL of media in each well was added either vehicle (DMSO), or a 20 mM stock solution of **c1**, **c2**, or DOX to give final concentrations of 10 or 20 μM drug and 0.1% DMSO. Live cell imaging was performed on a Zeiss Laser Scanning Confocal Microscope 880 with Airyscan (Oberkochen, Germany) with standard incubation conditions (37 °C, 5% CO_2, humidified), collecting images every 10 or 15 min for 18–24 h. Images were captured with a Plan-Apochromat 20x/0.8 air objective. DOX and the prodrugs were detected with excitation by a 458 nm laser at 0.3% and emission from 535 to 648 nm.

Each position consisted of a 3 slice z-stack that was compressed with a maximum intensity projection for analysis. Cells were identified using the cell count recipe from Aivia 9.8.1. The mean intensity for both channels was calculated, normalized, and then averaged to 30 min time points.

2.9. Cytotoxicity assays

H9C2 and 4T1 cells were plated at a density of 10,000 per well in 96-well plates. Twenty-four h after plating, cells were treated with 10 or 20 μM DOX (from 20 mM stock dissolved in DMSO, for 0.1% final DMSO) and were incubated for 24 or 48 h. The extracellular medium was centrifuged at 12,000×*g* for 5 min to pellet cellular debris, and the supernatants were assessed for release of lactate dehydrogenase (LDH) using a colorimetric activity assay (Invitrogen) as directed and spectral detection (Benchmark or BioRad microplate reader). Values were used to determine % cytotoxicity as described in the kit, using treatment with lysis buffer to release all LDH into the medium (defining 100% release) or cells without treatment (to define 0% release).

2.10. Western blot analysis

To evaluate levels of caspase cleavage (using an antibody recognizing both cleaved and uncleaved, Cell Signaling, cat#9662), Nrf2 (antibody from Thermo Fisher, cat#PA5-27882), and HO-1 (antibody from Proteintech, cat#10701-1-AP), H9C2 cells were plated at a density of 450,000 per well in a 24-well plate, then treated 24 h later with 10 or 20 μM DOX and incubated another 24 h before harvesting. For some samples, 100 mM hydroxocobalamin (HO-Cbl) was added 5 min before drug treatment. Cells were harvested by removing media (and recovering any non-adherent cells by centrifugation for 5 min at 10,600×*g*, discarding the supernatant), and combining that with the 120 μL of lysis buffer added to each well. Lysis buffer [50 mM Tris-HCl at pH 8.0, with 100 mM NaCl, 100 μM diethylene triamine pentaacetic acid (DTPA), 20 mM β-glycerophosphate, 0.1% SDS, 0.5% Na Desoxycholate, and 0.5% Triton-X-100] was prepared by freshly adding protease and phosphatase inhibitors before use (1 mM PMSF, 10 μg/mL aprotinin, 1 mM Na_3VO_4, 10 mM NaF and 10 μg/mL leupeptin). Samples were further incubated on ice for 30 min, then centrifuged at high speed (20,800×*g* for 10 min) to remove cell debris, and supernatants were mixed with 5X SDS protein sample buffer for Western blot analysis following resolution of 40 μg per sample on 10% SDS-polyacrylamide gels. Protein concentrations of supernatants were determined using a BCA assay (Pierce). Antibodies were used at dilutions of 1:1000 (for HO-1 and caspase-3) or 1:3000 (for Nrf2).

2.11. Statistical analysis

Data are presented as the mean ± standard error of the mean. Statistical analyses of data from LDH assays and Western blot intensity data (for caspase-3, Nrf2 and HO-1) were conducted by Student *t*-test. The criterion for statistical significance was set at $p < 0.05$.

3. Results and discussion

3.1. Chemical synthesis and characterization

3.1.1. Synthesis

We successfully accessed **c1** in a highly efficient, two-step synthesis (See Materials and Methods). Initially, we coupled 4-(hydroxymethyl) phenylboronic acid pinacol ester with di(2-pyridyl) thionocarbonate. The resulting activated thionocarbonate was treated with DOX and triethylamine to furnish **c1** in a 48% yield. As a control, we also generated **c2** via an analogous route. Like **c1**, **c2** was predicted to function as a H_2O_2-activated DOX prodrug. However, unlike **c1**, **c2** could not to liberate H_2S alongside DOX.

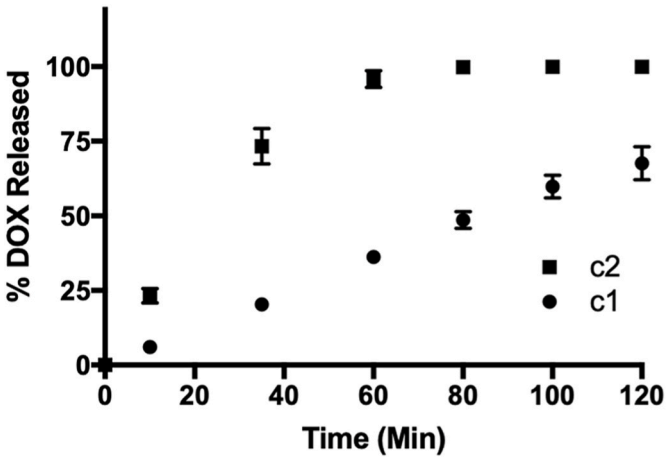

Fig. 3. Time-course for DOX release from prodrugs (10 μM) in ammonium bicarbonate buffer (0.1 M, pH 7.4) at room temperature and in the presence of H_2O_2 (10 μM). A calibration curve was used to determine the concentration of free DOX at each time point by LCMS. Plotted as the mean ± standard error of the mean (SEM) from three independent experiments.

3.1.2. Time-dependent DOX release from c1

Boronate oxidation is a bioorthogonal reaction that has been employed since the early 2000s to investigate the chemical biology of H_2O_2 under physiologically relevant conditions [43]. When the aryl boronate is linked to either an *S*- or *O*-alkyl thiocarbonate through the *para* position, this chemistry can be used to deliver carbonyl sulfide (COS), in response to elevated levels of ROS, via a 1,6-elimination [44]. Pluth and co-workers were the first to report on a small series of H_2S donors (via the ensuing enzyme-mediated hydrolysis of COS) using this chemistry [42]. Since this initial report, numerous examples have emerged in the literature [45–49], confirming this as a well-established approach for delivering H_2S under conditions of cellular oxidative stress. Therefore, with our strategic design of **c1**, it was predicted to undergo rapid boronate ester oxidation in the presence of H_2O_2, yielding a phenol which would then self-immolate to release both H_2S (via COS hydrolysis) and free DOX (Fig. 2B).

To confirm this reactivity, we incubated **c1** (10 μM) with H_2O_2 (10

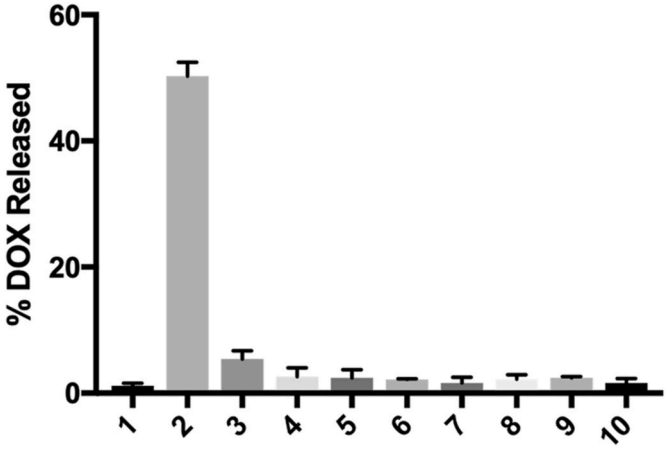

Fig. 4. Percentage of released DOX from c1 in response to various biological analytes during an 80 min incubation period at room temperature: (1) ammonium bicarbonate buffer (0.1 M, pH 7.5), (2) 10 μM H_2O_2, (3) 100 μM cysteine, (4) 100 μM homocysteine, (5) 1 mM glutathione, (6) 10 μM glutathione disulfide, (7) 10 μM sodium nitrite, (8) 10 μM sodium hypochlorite, (9) 10 μM superoxide, (10) 10 μM peroxynitrite. A calibration curve was used to determine the concentration of free DOX in response to each analyte. Plotted as the mean ± SEM from three independent experiments.

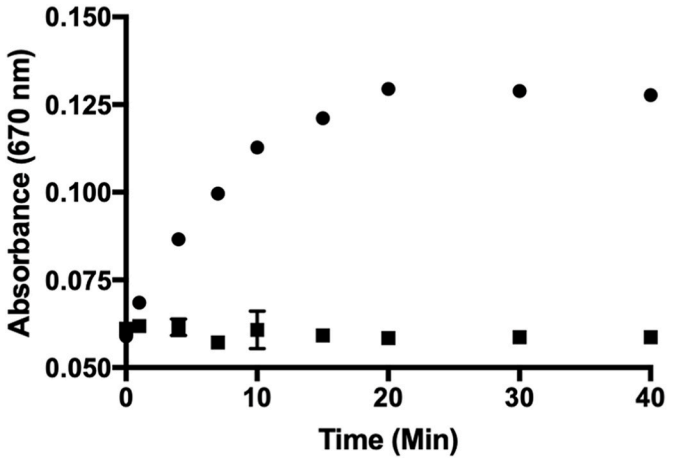

Fig. 5. Methylene blue assay depicting the time-dependent release of H_2S from c1 (40 μM) while in the presence of H_2O_2 (40 μM) and carbonic anhydrase (CA). Plotted as the mean ± SEM from three independent experiments. Data were collected in the presence (circles) or absence (squares) of H_2O_2.

μM) at room temperature in ammonium bicarbonate buffer (0.1 M, pH 7.4). At various time points, an aliquot was removed and analyzed by LCMS. Using a calibration curve, we determined the percentage of released DOX over the course of 2 h. As depicted in Fig. 3, **c1** displayed good reactivity towards peroxides, releasing free DOX in yield greater than 70% within the allotted time frame. For comparison, we also assessed the reactivity of **c2** towards the same concentration of peroxides. Like **c1**, **c2** also functioned as an H_2O_2-activated DOX prodrug, but with faster kinetics, as quantitative release of free DOX was realized within 60 min. This result, however, is not unexpected given that the carbamate functional group of **c2** is likely to increase rates of both the 1,6-elimination and the breakdown of the ensuing carbamic acid to liberate CO_2 and free DOX [45]. However, the slow and sustained release of DOX from **c1**, confirmed its potential to serve as an H_2O_2-activated, bifunctional prodrug.

3.1.3. *Selectivity of c1*

To assess selectivity, **c1** was incubated with various biological analytes at room temperature and in ammonium bicarbonate buffer (0.1 M, pH 7.4). After a reaction time of 80 min, an aliquot was removed and analyzed by LC-MS. As highlighted in Fig. 4, **c1** was shown to be relatively stable in buffer alone and while in the presence of reductants (cysteine, homocysteine, and glutathione) and other oxidants (glutathione disulfide, sodium nitrite, sodium hypochlorite, superoxide, and peroxynitrite). In fact, other than small amounts of DOX, only the boronic acid derivative of **c1** was observed (as expected and due to hydrolysis of the pinacol boronate ester) by LC-MS, highlighting the overall stability of the prodrug. However, in the presence of H_2O_2, significant levels of free DOX were observed by LC-MS. Collectively, these

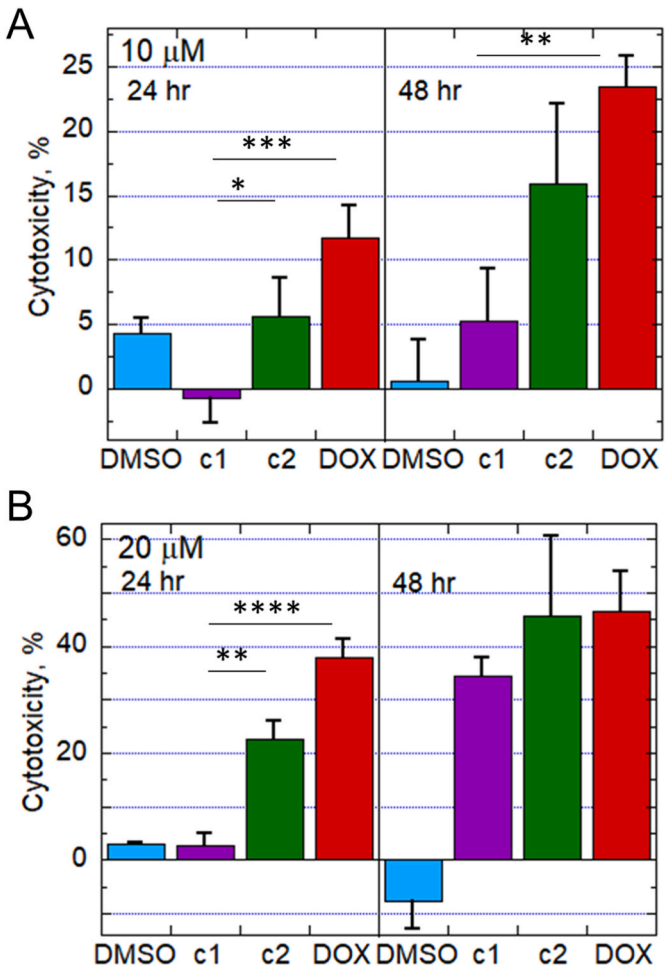

Fig. 7. Cytotoxicity of DOX and prodrugs in H9C2 cardiomyoblasts. Media from cells exposed for 24 or 48 h to 10 or 20 μM (A and B, respectively) of **c1**, **c2**, DOX or vehicle (DMSO, final concentration 0.1% in all samples) was centrifuged to remove cells and cell debris, and supernatants were assessed spectrophotometrically by lactose dehydrogenase (LDH) assay to evaluate release into the media as a measure of cytotoxicity (n = 6 or more). *, $p < 0.05$; **, $p < 0.01$; ***, $p < 0.001$; ****, $p < 0.0001$.

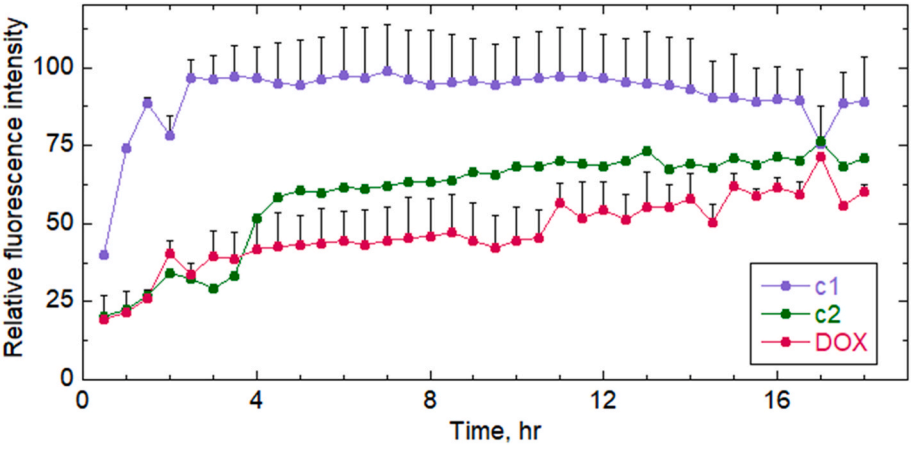

Fig. 6. Uptake of DOX and prodrugs **c1** and **c2** by H9C2 cardiomyoblasts. H9C2 cells cultures grown overnight on chambered coverslips in media with 10% serum were switched to Fluorobrite DMEM imaging media supplemented with 5% serum and prepared for live-cell imaging on a Zeiss LSM 880 confocal microscope, then 10 μM of **c1**, **c2**, or DOX was added and images were taken every 10 min (averaged every 30 min) for 18 h. Approximately 20 cells present in each field of view were averaged for each sample and time point; normalized and averaged data from two replicates each ± SEM were included for **c1** and DOX. An earlier independent trial yielded very similar results (Fig. S4).

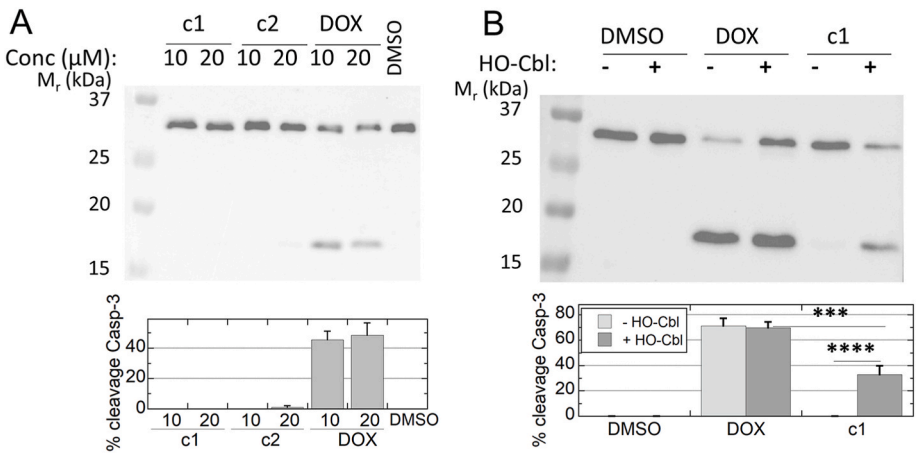

Fig. 8. Caspase cleavage monitored by an antibody against total caspase-3 demonstrates the H_2S -dependent protection exhibited by **c1** against DOX-mediated apoptotic signaling. H9C2 cells in culture were treated for 24 h with **c1**, **c2**, DOX or vehicle (DMSO), then harvested into lysis buffer and immunoblotted for caspase-3. Data analyzed by ImageJ were used to assess the percent of the two bands present as the lower band. A. At 24 h, only DOX treatment causes caspase-3 cleavage (n = 3). B. When 100 mM hydroxocobalamin is added 5 min prior to 10 μM drug treatments, **c1**-treated cells exhibit much more cleavage of caspase-3 than in its absence, whereas cleavage due to DOX treatment is unchanged (n = 7); ***, $p < 0.001$; ****, $p < 0.0001$.

results underscore the superb selectivity of **c1** and confirm our proposed mechanism for its release of DOX, as shown in Fig. 2B.

3.1.4. H_2S release from c1

We confirmed the time-dependent liberation of H_2S using a methylene blue assay [50] and measuring the resulting absorbance at 670 nm after **c1** exposure to H_2O_2 (Fig. 5, circles). Using a calibration curve generated with Na_2S, we determined that **c1** (40 μM) was able to release more than 16 μM H_2S while in the presence of both H_2O_2 (40 μM) and carbonic anhydrase (CA). Conversely, negligible amounts of H_2S were observed in the absence of peroxides (Fig. 5, squares). As a control, the same assay was also run in the absence of CA (Fig. S3). Under these conditions, **c1** exposure to H_2O_2 yielded small amounts of H_2S (<5 μM). This is presumably due to isocyanate formation and the direct release of H_2S from the breakdown of **4** (Fig. 2B and Fig. S4) [45]. Therefore, these results not only confirm the efficient release of H_2S from **c1** under conditions of oxidative stress, but they also verify that the predominant route of H_2S production (~70%) is via COS hydrolysis facilitated by CA (Fig. 2B).

3.2. Biological analyses

3.2.1. Uptake of DOX and prodrugs into H9C2 cardiomyoblasts

Before comparing the biological effects of treatments by DOX and prodrugs, it was important to know their time dependence of accumulation into the H9C2 cardiomyoblasts under investigation. DOX and the prodrugs are fluorescent and can therefore be tracked as they accumulate in cells over time using confocal microscopy of live cells in culture, allowing direct comparisons between **c1**, **c2** and DOX. In two trials shown in Fig. 6 and Fig. S5, **c1** accumulated rapidly in cells (giving maximal signal by ~ 2 h) compared with DOX. On the other hand, **c2** was similar to DOX in being taken up relatively slowly by these cells. Thus, any biological effects observed using **c1** rather than DOX will not be due to limited cellular uptake.

3.2.2. H_2S-dependent suppression of DOX-mediated cytotoxicity in H9C2 cells by c1 compared with c2 or the parent drug, DOX

Cytotoxicity of **c1**, **c2** and DOX was evaluated by measuring the release of lactate dehydrogenase (LDH) into the culture medium over time. Even though **c1** was the fastest to accumulate in cells based on our confocal microscopy data (Fig. 6), DOX was more toxic than **c1** at both doses, 10 and 20 μM. However, the difference was not significant at the longer exposure time (48 h) (Fig. 7). On the other hand, **c2**, which releases DOX but not H_2S and is slow to enter cells, was not significantly less toxic than DOX.

Parallel studies utilizing murine 4T1 triple-negative breast cancer cells grown in culture were conducted as a preliminary test to see if **c1** could retain the cytotoxic properties of DOX to support its use as a chemotherapeutic agent. We found that, other than the lowest dose and shortest time, where toxicity is minimal for all compounds, **c1** exhibits comparable toxicity relative to DOX in 4T1 cells, perhaps owing to the anticancer activity of H_2S in combination with DOX (Fig. S6).

3.2.3. H_2S-dependence of the decreased cytotoxicity of c1 in H9C2 cells

We next evaluated apoptotic signaling through caspase-3 cleavage at 24 h to compare the experimental compounds. Unlike DOX, neither **c1**

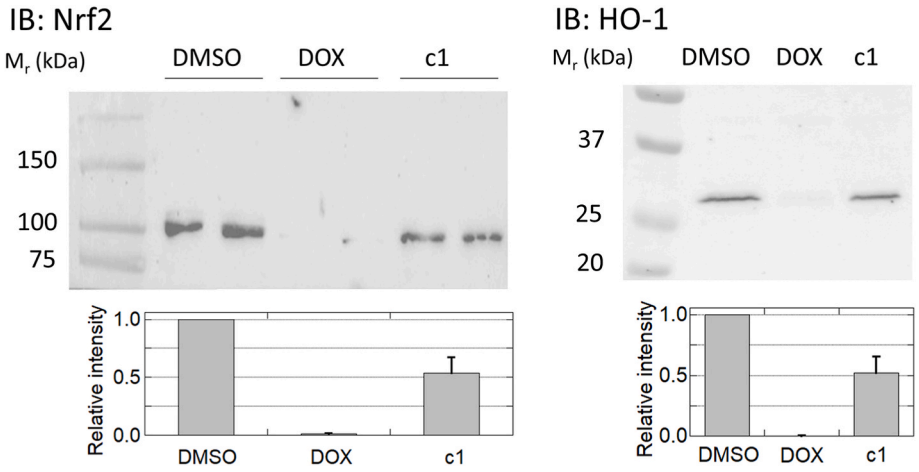

Fig. 9. **c1**-treated cardiomyoblasts do not shut down Nrf2 activation as DOX does. Immunoblots for the transcriptional regulator Nrf2 (left) and one of its downstream targets, HO-1 (right), demonstrate stabilization of Nrf2 with concomitant expression of HO-1 in DMSO-treated samples; DOX treatment completely suppressed both, while **c1** treatment was only moderately suppressive (n = 4 and n = 3 for Nrf2 and HO-1, respectively). The bar graphs below represent the mean ± SEM. Results were statistically different between **c1** and DOX in both cases ($p = 0.002$ and $p = 0.019$), and more marginally so between **c1** and DMSO ($p = 0.011$ and p. = 0.025), for Nrf2 and HO-1, respectively.

nor **c2** at either 10 or 20 μM caused notable caspase-3 cleavage within 24 h (Fig. 8a). Use of a scavenger of H_2S, hydroxocobalamin (HO-Cbl) [51], provided evidence that the protective effect of this DOX-releasing prodrug, **c1**, is substantially dependent on its ability to release H_2S (Fig. 8b).

3.2.4. Preservation of nuclear factor erythroid 2-related factor 2 (Nrf2) activation and antioxidant enzyme (HO-1) expression by c1, but not DOX, in H9C2 cells

Nrf2 is a known transcriptional regulator activated when Keap-1 senses oxidants and electrophiles, leading to induced expression of antioxidant enzymes; activation of Nrf2 is a key factor in cardioprotection from anthracycline toxicity *in vivo* [52,53]. Our data using DOX-treated cardiomyoblasts, consistent with studies by others [54,55], confirmed the suppression of both Nrf2 activation and expression of a downstream target, heme-oxygenase 1 (HO-1), relative to the vehicle control; **c1**, on the other hand, largely preserved Nrf2 activation and HO-1 expression, indicating that activation of the Nrf2 transcriptome is a likely mechanism involved in the protection of cardiomyoblasts against toxicity observed by treatment with **c1** rather than DOX (Fig. 9).

4. Conclusions

In this study, we disclosed a novel hybrid prodrug (**c1**) that was shown to selectively release both DOX and H_2S upon exposure to H_2O_2. We found that **c1** accumulates relatively rapidly in cardiomyoblasts but has diminished apoptotic effects compared with DOX, dependent upon its release of H_2S. These **c1**-treated cells exhibit higher Nrf2 and HO1 levels than DOX-treated cells. Preliminary indications, using a mouse triple-negative breast cancer cell line sensitive to DOX treatment, are that **c1** maintains toxicity against this cell line, although with somewhat altered time dependence that may stem, in part, from its facile accumulation in cells. Although not a part of the present study, it has been shown that H_2S production concomitant with DOX release impeded efflux of the drug from a DOX-resistant sarcoma cell line, suggesting selectively toxic effects of H_2S co-production on some treatment-resistant cancers [21]. Taken together, our results indicate that DOX prodrugs that impart tumor-selective activation by ROS such as H_2O_2, along with H_2S delivery, provide a highly promising and synergistic strategy for combating DOX-induced cardiotoxicity. The impact and significance of this new design strategy will be further evaluated in an *in vivo* mouse model and disclosed in due course.

Funding sources

Research presented was supported in part by pilot grants from the Center for Redox Biology and Medicine (CRBM) and the Center for Molecular Signaling (CMS) to J.C.L. and L.B.P., by R35 GM135179 to L. B.P., and by the National Science Foundation (Grant No. 2143826) to J. C.L.

Author contributions

J.C.L. designed the **c1** and **c2** compounds and the synthetic approaches, and supervised the synthetic and characterization work that was conducted by Q.H. R.D.Y. conducted the biological assays of **c1** and **c2** under the supervision of L.B.P., and H.B.-H. performed the confocal microscopy experiments. J.C.L. and L.B.P. drafted and edited the manuscript, and D.R.S.-P. shared biological materials and provided critical intellectual feedback for the overall project.

Declaration of competing interest

The authors declare the following financial interests/personal relationships which may be considered as potential competing interests: John C. Lukesh reports financial support was provided by National Science Foundation. Leslie B. Poole reports financial support was provided by National Institute of General Medical Sciences. John C. Lukesh and Leslie B. Poole have a provisional patent pending to Wake Forest University.

Appendix A. Supplementary data

Supplementary data to this article can be found online at https://doi.org/10.1016/j.redox.2022.102338.

References

[1] G. Minotti, P. Menna, E. Salvatorelli, G. Cairo, L. Gianni, Anthracyclines: molecular advances and pharmacologic developments in antitumor activity and cardiotoxicity, Pharmacol. Rev. 56 (2) (2004) 185–229, https://doi.org/10.1124/pr.56.2.6.

[2] F. Arcamone, G. Cassinelli, G. Fantini, A. Grein, P. Orezzi, C. Pol, C. Spalla, Adriamycin, 14-hydroxydaimomycin, a new antitumor antibiotic FromS. Peucetius Var.Caesius, Biotechnol. Bioeng. 11 (6) (1969) 1101–1110, https://doi.org/10.1002/bit.260110607.

[3] J. Sun, Q. Wei, Y. Zhou, J. Wang, Q. Liu, H. Xu, A systematic analysis of FDA-approved anticancer drugs, BMC Syst. Biol. 11 (S5) (2017) 87, https://doi.org/10.1186/s12918-017-0464-7.

[4] S. Sritharan, N. Sivalingam, A comprehensive review on time-tested anticancer drug doxorubicin, Life Sci. 278 (2021) 119527, https://doi.org/10.1016/j.lfs.2021.119527.

[5] D.A. Gewirtz, Critical evaluation of the mechanisms of action proposed for the antitumor effects of the anthracycline antibiotics adriamycin and daunorubicin, Biochem. Pharmacol. 57 (7) (1999) 727–741, https://doi.org/10.1016/S0006-2952(98)00307-4.

[6] P.K. Singal, N. Iliskovic, Doxorubicin-induced cardiomyopathy, N. Engl. J. Med. 339 (13) (1998) 900–905, https://doi.org/10.1056/NEJM199809243391307.

[7] A.U. Buzdar, C. Marcus, G.R. Blumenschein, T.L. Smith, Early and delayed clinical cardiotoxicity of doxorubicin, Cancer 55 (12) (1985) 2761–2765, https://doi.org/10.1002/1097-0142(19850615)55:12<2761::AID-CNCR2820551206>3.0.CO;2-P.

[8] S.M. Swain, F.S. Whaley, M.S. Ewer, Congestive heart failure in patients treated with doxorubicin: a retrospective analysis of three trials, Cancer 97 (11) (2003) 2869–2879, https://doi.org/10.1002/cncr.11407.

[9] J.M. Berthiaume, K.B. Wallace, Adriamycin-induced oxidative mitochondrial cardiotoxicity, Cell Biol. Toxicol. 23 (1) (2007) 15–25, https://doi.org/10.1007/s10565-006-0140-y.

[10] S. Granados-Principal, J.L. Quiles, C.L. Ramirez-Tortosa, P. Sanchez-Rovira, Mc Ramirez-Tortosa, New advances in molecular mechanisms and the prevention of adriamycin toxicity by antioxidant nutrients, Food Chem. Toxicol. 48 (6) (2010) 1425–1438, https://doi.org/10.1016/j.fct.2010.04.007.

[11] Y. Octavia, C.G. Tocchetti, K.L. Gabrielson, S. Janssens, H.J. Crijns, A.L. Moens, Doxorubicin-induced cardiomyopathy: from molecular mechanisms to therapeutic strategies, J. Mol. Cell. Cardiol. 52 (6) (2012) 1213–1225, https://doi.org/10.1016/j.yjmcc.2012.03.006.

[12] S. Upadhayay, N. Sharma, A.K. Mantha, M. Dhiman, ANTI-CANCER drug doxorubicin induced cardiotoxicity: understanding the mechanisms involved IN ROS generation resulting IN mitochondrial dysfunction, Rasayan J. Chem. 13 (2020) 1042–1053, https://doi.org/10.31788/RJC.2020.1325603, 02.

[13] P.S. Rawat, A. Jaiswal, A. Khurana, J.S. Bhatti, U. Navik, Doxorubicin-induced cardiotoxicity: an update on the molecular mechanism and novel therapeutic strategies for effective management, Biomed. Pharmacother. 139 (2021) 111708, https://doi.org/10.1016/j.biopha.2021.111708.

[14] J.H. Doroshow, K.J. Davies, Redox cycling of anthracyclines by cardiac mitochondria. II. Formation of superoxide anion, hydrogen peroxide, and hydroxyl radical, J. Biol. Chem. 261 (7) (1986) 3068–3074, https://doi.org/10.1016/S0021-9258(17)35747-2.

[15] K.B. Wallace, V.A. Sardão, P.J. Oliveira, Mitochondrial determinants of doxorubicin-induced cardiomyopathy, Circ. Res. 126 (7) (2020) 926–941, https://doi.org/10.1161/CIRCRESAHA.119.314681.

[16] J.H. Doroshow, G.Y. Locker, C.E. Myers, Enzymatic defenses of the mouse heart against reactive oxygen metabolites, J. Clin. Invest. 65 (1) (1980) 128–135, https://doi.org/10.1172/JCI109642.

[17] J. Quiles, Antioxidant nutrients and adriamycin toxicity, Toxicology 180 (1) (2002) 79–95, https://doi.org/10.1016/S0300-483X(02)00383-9.

[18] S.M. DeAtley, M.Y. Aksenov, M.V. Aksenova, B. Harris, R. Hadley, P. Cole Harper, J.M. Carney, D.A. Butterfield, Antioxidants protect against reactive oxygen species associated with adriamycin-treated cardiomyocytes, Cancer Lett. 136 (1) (1999) 41–46, https://doi.org/10.1016/S0304-3835(98)00306-1.

[19] K. Hideg, T. Kálai, Novel antioxidants in anthracycline cardiotoxicity, Cardiovasc. Toxicol. 7 (2) (2007) 160–164, https://doi.org/10.1007/s12012-007-0019-z.

[20] K. Chegaev, C. Riganti, B. Rolando, L. Lazzarato, E. Gazzano, S. Guglielmo, D. Ghigo, R. Fruttero, A. Gasco, Doxorubicin-antioxidant Co-drugs, Bioorg. Med. Chem. Lett 23 (19) (2013) 5307–5310, https://doi.org/10.1016/j.bmcl.2013.07.070.

[21] K. Chegaev, B. Rolando, D. Cortese, E. Gazzano, I. Buondonno, L. Lazzarato, M. Fanelli, C.M. Hattinger, M. Serra, C. Riganti, R. Fruttero, D. Ghigo, A.H. Gasco, $_2$ S-donating doxorubicins may overcome cardiotoxicity and multidrug resistance,

J. Med. Chem. 59 (10) (2016) 4881–4889, https://doi.org/10.1021/acs.jmedchem.6b00184.
[22] J.M. Fukuto, S.J. Carrington, D.J. Tantillo, J.G. Harrison, L.J. Ignarro, B. A. Freeman, A. Chen, D.A. Wink, Small molecule signaling agents: the integrated chemistry and biochemistry of nitrogen oxides, oxides of carbon, dioxygen, hydrogen sulfide, and their derived species, Chem. Res. Toxicol. 25 (4) (2012) 769–793, https://doi.org/10.1021/tx2005234.
[23] X. Cao, L. Ding, Z. Xie, Y. Yang, M. Whiteman, P.K. Moore, J.-S. Bian, A review of hydrogen sulfide synthesis, metabolism, and measurement: is modulation of hydrogen sulfide a novel therapeutic for cancer? Antioxidants Redox Signal. 31 (1) (2019) 1–38, https://doi.org/10.1089/ars.2017.7058.
[24] H. Kimura, Hydrogen sulfide: its production, release and functions, Amino Acids 41 (1) (2011) 113–121, https://doi.org/10.1007/s00726-010-0510-x.
[25] M. Bhatia, Hydrogen sulfide as a vasodilator, IUBMB Life Int. Union Biochem. Mol. Biol. Life 57 (9) (2005) 603–606, https://doi.org/10.1080/15216540500217875.
[26] S. Cacanyiova, A. Berenyiova, F. Kristek, The role of hydrogen sulphide in blood pressure regulation, Physiol. Res. S273–S289 (2016), https://doi.org/10.33549/physiolres.933438.
[27] M.R. Filipovic, J. Zivanovic, B. Alvarez, R. Banerjee, Chemical biology of H_2S signaling through persulfidation, Chem. Rev. 118 (3) (2018) 1253–1337, https://doi.org/10.1021/acs.chemrev.7b00205.
[28] W. Zhao, The vasorelaxant effect of H2S as a novel endogenous gaseous KATP channel opener, EMBO J. 20 (21) (2001) 6008–6016, https://doi.org/10.1093/emboj/20.21.6008.
[29] J.W. Elrod, J.W. Calvert, J. Morrison, J.E. Doeller, D.W. Kraus, L. Tao, X. Jiao, R. Scalia, L. Kiss, C. Szabo, H. Kimura, C.-W. Chow, D.J. Lefer, Hydrogen sulfide attenuates myocardial ischemia-reperfusion injury by preservation of mitochondrial function, Proc. Natl. Acad. Sci. Unit. States Am. 104 (39) (2007) 15560–15565, https://doi.org/10.1073/pnas.0705891104.
[30] D. Johansen, K. Ytrehus, G.F. Baxter, Exogenous hydrogen sulfide (H2S) protects against regional myocardial ischemia–reperfusion injury: evidence for a role of KATP channels, Basic Res. Cardiol. 101 (1) (2006) 53–60, https://doi.org/10.1007/s00395-005-0569-9.
[31] E.M. Bos, H. van Goor, J.A. Joles, M. Whiteman, H.G.D. Leuvenink, Hydrogen sulfide: physiological properties and therapeutic potential in ischaemia: properties of H_2S in ischaemia, Br. J. Pharmacol. 172 (6) (2015) 1479–1493, https://doi.org/10.1111/bph.12869.
[32] M.K. Muellner, S.M. Schreier, H. Laggner, M. Hermann, H. Esterbauer, M. Exner, B. M.K. Gmeiner, S. Kapiotis, Hydrogen sulfide destroys lipid hydroperoxides in oxidized LDL, Biochem. J. 420 (2) (2009) 277–281, https://doi.org/10.1042/BJ20082421.
[33] N. Panth, K.R. Paudel, K. Parajuli, Reactive oxygen species: a key hallmark of cardiovascular disease, Adv. Met. Med. 2016 (2016) 1–12, https://doi.org/10.1155/2016/9152732.
[34] K. Sugamura, J.F. Keaney, Reactive oxygen species in cardiovascular disease, Free Radic. Biol. Med. 51 (5) (2011) 978–992, https://doi.org/10.1016/j.freeradbiomed.2011.05.004.
[35] J. Peiró Cadahía, V. Previtali, N.S. Troelsen, M.H. Clausen, Prodrug strategies for targeted therapy triggered by reactive oxygen species, MedChemComm 10 (9) (2019) 1531–1549, https://doi.org/10.1039/C9MD00169G.
[36] G.-Y. Liou, P. Storz, Reactive oxygen species in cancer, Free Radic. Res. 44 (5) (2010) 479–496, https://doi.org/10.3109/10715761003667554.
[37] L. Wang, S. Xie, L. Ma, Y. Chen, W. Lu, 10-Boronic acid substituted camptothecin as prodrug of SN-38, Eur. J. Med. Chem. 116 (2016) 84–89, https://doi.org/10.1016/j.ejmech.2016.03.063.
[38] Y. Kuang, K. Balakrishnan, V. Gandhi, X. Peng, Hydrogen peroxide inducible DNA cross-linking agents: targeted anticancer prodrugs, J. Am. Chem. Soc. 133 (48) (2011) 19278–19281, https://doi.org/10.1021/ja2073824.
[39] Y. Ai, O.N. Obianom, M. Kuser, Y. Li, Y. Shu, F. Xue, Enhanced tumor selectivity of 5-fluorouracil using a reactive oxygen species-activated prodrug approach, ACS Med. Chem. Lett. 10 (1) (2019) 127–131, https://doi.org/10.1021/acsmedchemlett.8b00539.
[40] C. Skarbek, S. Serra, H. Maslah, E. Rascol, R. Labruère, Arylboronate prodrugs of doxorubicin as promising chemotherapy for pancreatic cancer, Bioorg. Chem. 91 (2019) 103158, https://doi.org/10.1016/j.bioorg.2019.103158.
[41] A.K. Steiger, S. Pardue, C.G. Kevil, M.D. Pluth, Self-immolative thiocarbamates provide access to triggered H_2S donors and analyte replacement fluorescent probes, J. Am. Chem. Soc. 138 (23) (2016) 7256–7259, https://doi.org/10.1021/jacs.6b03780.
[42] Y. Zhao, M.D. Pluth, Hydrogen sulfide donors activated by reactive oxygen species, Angew. Chem. Int. Ed. 55 (47) (2016) 14638–14642, https://doi.org/10.1002/anie.201608052.
[43] A.R. Lippert, G.C. Van de Bittner, C.J. Chang, Boronate oxidation as a bioorthogonal reaction approach for studying the chemistry of hydrogen peroxide in living systems, Acc. Chem. Res. 44 (9) (2011) 793–804, https://doi.org/10.1021/ar200126t.
[44] C.M. Levinn, M.M. Cerda, M.D. Pluth, Development and application of carbonyl sulfide-based donors for H2S delivery, Acc. Chem. Res. 52 (9) (2019) 2723–2731.
[45] Y. Zhao, H.A. Henthorn, M.D. Pluth, Kinetic insights into hydrogen sulfide delivery from caged-carbonyl sulfide isomeric donor platforms, J. Am. Chem. Soc. 139 (2017) 16365–16376.
[46] M. Yao, Y. Lu, L. Shi, Y. Huang, Q. Zhang, J. Tan, P. Hu, J. Zhang, G. Luo, N. A. Zhang, ROS-responsive, self-immolative and self-reporting hydrogen sulfide donor with multiple biological activities for the treatment of myocardial infarction, Bioact. Mater. 9 (2022) 168–182.
[47] Y. Hu, X. Li, Y. Fang, W. Shi, X. Li, W. Chen, M. Xian, H. Ma, Reactive oxygen species-triggered off-on fluorescence donor for imaging hydrogen sulfide delivery in living cells, Chem. Sci. 10 (2019) 7690–7694.
[48] P. Chauhan, S. Jos, H. Chakrapani, Reactive oxygen species-triggered tunable hydrogen sulfide release, Org. Lett. 20 (13) (2018), 3776–3770.
[49] C. Zhu, S.I. Suarez, J.C. Lukesh, Illuminating and alleviating cellular oxidative stress with an ROS-activated, H2S-donating theranostic, Tetrahedron Lett. 69 (2021) 152944–152948.
[50] M.D. Hartle, M.D. Pluth, A practical guide to working with H_2S at the interface of chemistry and biology, Chem. Soc. Rev. 45 (22) (2016) 6108–6117, https://doi.org/10.1039/C6CS00212A.
[51] D.H. Truong, A. Mihajlovic, P. Gunness, W. Hindmarsh, P.J. O'Brien, Prevention of hydrogen sulfide (H2S)-Induced mouse lethality and cytotoxicity by hydroxocobalamin (vitamin B12a), Toxicology 242 (1–3) (2007) 16–22, https://doi.org/10.1016/j.tox.2007.09.009.
[52] S. Mirzaei, A. Zarrabi, F. Hashemi, A. Zabolian, H. Saleki, N. Azami, S. Hamzehlou, M.V. Farahani, K. Hushmandi, M. Ashrafizadeh, H. Khan, A.P. Kumar, Nrf2 signaling pathway in chemoprotection and doxorubicin resistance: potential application in drug discovery, Antioxid. Basel Switz. 10 (3) (2021) 349, https://doi.org/10.3390/antiox10030349.
[53] K.K.S. Nordgren, K.B. Wallace, Disruption of the Keap1/nrf2-antioxidant response system After chronic doxorubicin exposure in vivo, Cardiovasc. Toxicol. 20 (6) (2020) 557–570, https://doi.org/10.1007/s12012-020-09581-7.
[54] A.M. Alzahrani, P. Rajendran, V.P. Veeraraghavan, H. Hanieh, Cardiac protective effect of Kirenol against doxorubicin-induced cardiac hypertrophy in H9c2 cells through Nrf2 signaling via PI3K/AKT pathways, Int. J. Mol. Sci. 22 (6) (2021) 3269, https://doi.org/10.3390/ijms22063269.
[55] J. Gu, H. Huang, C. Liu, B. Jiang, M. Li, L. Liu, S. Zhang, Pinocembrin inhibited cardiomyocyte pyroptosis against doxorubicin-induced cardiac dysfunction via regulating nrf2/sirt3 signaling pathway, Int. Immunopharm. 95 (2021) 107533, https://doi.org/10.1016/j.intimp.2021.107533.